Chemical Synthesis and Structural and Magnetic Properties of Dispersible Cobalt-and Nickel-Doped ZnO Nanocrystals

ARTICLE *in* THE JOURNAL OF PHYSICAL CHEMISTRY C · MARCH 2010

Impact Factor: 4.77 · DOI: 10.1021/jp9105579

Chemical Synthesis and Structural and Magnetic Properties of Dispersible Cobalt- and Nickel-Doped ZnO Nanocrystals

Anshu Singhal,*,† S. N. Achary,† J. Manjanna,‡ S. Chatterjee,§ P. Ayyub,§ and A. K. Tyagi†

Chemistry Division, Bhabha Atomic Research Centre, Mumbai-400 085, India, Department of Systems Innovation, School of Engineering, University of Tokyo, Japan, and Department of Condensed Matter Physics, Tata Institute of Fundamental Research, Mumbai-400 005 India

Received: November 5, 2009; Revised Manuscript Received: January 13, 2010

The preparation, characterization, and magnetic properties of dispersible Co- and Ni-doped ZnO nanocrystals (NC) are reported. The nanocrystals, $Zn_{1-x}TM_xO$ where $x = 0-0.07$ for TM = Co and $x = 0.02, 0.03$ for TM = Ni have been synthesized by nonhydrolytic alcoholysis esterification elimination reaction using anhydrous metal carboxylates as precursors in the presence of oleic acid and oleyl alcohol at temperatures as low as 220 °C. The prepared nanocrystals can be easily dispersed in solvents like chloroform and toluene. Detailed X-ray diffraction (XRD) using synchrotron radiation (SR), microstructure, and Raman studies reveal that the Co-doped ZnO nanocrystals are single-phase wurtzite structure without any parasitic secondary phases and Co atoms are incorporated into the ZnO lattice and located at the substitutional sites of the Zn atoms. Magnetic studies as a function of temperature and field indicate that Co- and Ni-doped zinc oxide nanocrystals are ferromagnetic at room temperature (RT). The observed ferromagnetism in Co-doped ZnO nanocrystals is interpreted in terms of a spin-split donor impurity-band model. The detection of donor defects bound to Co sites by Raman spectroscopy and decreased magnetization in oxygen-annealed samples suggest that activation of ferromagnetism depends on defects, such as oxygen vacancies (V_O) and zinc interstitials (Zn_i). On the other hand, the observation of secondary phases like NiO and Ni in the powder XRD patterns of Ni-doped ZnO nanocrystals suggests the extrinsic origin of ferromagnetism in this material.

Introduction

Diluted magnetic semiconductors (DMSs) have recently attracted broad interest for their promise in the emerging field of spintronics.[1,2] The major aim in realizing spintronic devices is to develop DMSs with room-temperature ferromagnetism.[3] Optically transparent ferromagnetic DMSs, obtained by doping transition metal (TM) ions into wide band gap semiconductors, have received particular attention for integrated optospintronic applications.[4,5] Specifically, ZnO, which has large band gap and exciton binding energies, excellent mechanical characteristics, and is inexpensive and environmentally safe, has been identified as a promising host material after computational studies have predicted ferromagnetism above room temperature for several ZnO-based DMSs.[6] The experimental results regarding room-temperature ferromagnetism (rtfm) in the ZnO/Co system in thin films, bulk, and polycrystalline samples, however, differ widely with the properties of such materials depending highly on the methods of syntheses employed. For example, Ueda et al.[7] found Co-doped ZnO films prepared by pulsed laser deposition (PLD) to be ferromagnetic above 280 K. $Zn_{1-x}Co_xO$ films obtained by the sol−gel method were also found to be ferromagnetic with a $T_C > 300$ K by Lee et al.,[8] although the presence of secondary phase was noted in the samples $x \geq 0.25$. Some groups observe rtfm in the absence of secondary phases or cobalt clusters.[9–11] However, others report no ferromagnetism at room temperature[12] or that the observed ferromagnetism originates from metallic cobalt clusters.[13] Schwartz et al.[14] report intrinsic ferromagnetism in colloidal Co^{2+}-doped ZnO nanocrystals, which they attribute to the presence of interface defects. X-ray magnetic circular dichroism (XMCD) measurements have shown that dissolved cobalt atoms produce purely paramagnetic behavior, but that a ferromagnetic component is present, which is possible from defects created in the material.[15]

Some studies have explained the importance of carriers and defects in mediating ferromagnetism in ZnO. Tuan et al.[16] found that weak ferromagnetism in Co-doped ZnO films can be activated by postgrowth vacuum annealing, changing the films from insulating to semiconducting behavior. The specific role of zinc interstitials (Zn_i), which are believed to form a shallow donor state in ZnO, has also been studied. Reversible on/off ferromagnetic ordering at room temperature in chemically synthesized Co-doped ZnO films was achieved by the controlled incorporation and removal of Zn_i.[17a] Khare et al.[17b] also found that the magnetization in Co-doped ZnO is enhanced by introducing Zn_i into the lattice during annealing. All these studies suggest that ferromagnetism in Co-doped ZnO is highly dependent on intrinsic defects in the material. These defects may rely on the presence of the transition metal dopants by the formation of complexes that mediate FM ordering, or defects alone may be enough to cause ferromagnetism, such as that reported for undoped HfO_2.[18]

The experimental situation of the Ni-doped ZnO system is similar to that of Co-doped ZnO. In Ni-doped ZnO films prepared by the PLD technique, ferromagnetism at 2 K has been reported,[19] whereas above 30 K, superparamagnetic behavior was observed. Yin et al.[20] reported paramagnetism in the Ni-doped ZnO films. On the other hand, room-temperature ferromagnetism has been reported for Ni-doped ZnO nanorods,[21] films,[10a] and nanowires arrays.[22] There are further reports that

* To whom correspondence should be addressed. E-mail: ansing@barc.gov.in.
† Bhabha Atomic Research Centre.
‡ University of Tokyo.
§ Tata Institute of Fundamental Research.

10.1021/jp9105579
Published on Web 02/04/2010

Ni-doped ZnO quantum dots prepared by a wet chemical method may be a good DMS material with ferromagnetism up to 350 K.[23–25]

The origin of ferromagnetism in magnetically doped semiconductor materials has long been under debate. Many theories have been proposed, such as superexchange, double exchange between the d states of TMs, free-carrier-mediated exchange, and sp−d exchange mechanism, etc.[26] Coey et al.[27] have proposed another model for ferromagnetism in oxide-based DMS materials based on a spin-split donor impurity band. In the model, donor defects (which could arise from either oxygen vacancies (V_O) or Zn_i in the case of ZnO) overlap at large concentrations to form a donor impurity band. The impurity band can interact with local magnetic moments through the formation of bound magnetic polarons (BMP). Within each BMP, the bound carrier interacts with the magnetic dopants inside its radius and can align the spins of the magnetic dopants parallel to one another. Ferromagnetism is achieved when the BMPs start to overlap to form a continuous chain throughout the material, thus percolating ferromagnetism in the DMS.

The above discussion suggests that understanding and controlling ferromagnetic ordering in DMSs is still a significant challenge. Further, the observance of wide range of magnetic properties displayed by the ZnO DMSs prepared by different methods emphasizes the need to develop reproducible methods for preparing high-T_C ferromagnetic DMSs. Many proposed spintronics devices involve DMSs of nanometer dimensions,[28] and the solution syntheses provide the opportunity to study free-standing DMS crystals in this size regime. The solution phase preparations of colloidal nanocrystals (NCs) are performed under milder conditions in comparison to typical solid-state synthetic methods and allow for a uniform diffusion of reactants during the nanocrystal growth. Because of small sizes of free-standing NCs, the formation of secondary phases within individual NCs is not likely. Furthermore, colloidal NCs can be used as building blocks for the bottom-up assembly of functional devices.[29]

In this paper, we report a facile, high-yield, chemical synthesis of colloidal Co- and Ni-doped ZnO nanocrystals using anhydrous metal carboxylates as precursors in the presence of oleic acid and oleyl alcohol which act as reactants as well as control agents for particle growth, their detailed structural characterization, and magnetic properties.

Experimental Details

Zinc acetate (99.99%, Aldrich), cobalt acetate (99.99%, Aldrich), oleic acid (97%, Acros), and oleyl alcohol (85%, Aldrich) were used as received. Anhydrous nickel acetate was obtained by drying the nickel acetate tetrahydrate (99.998%, Aldrich) in a vacuum oven at 90 °C to a constant mass.[30] All the experiments were carried out using standard oxygen-free techniques under argon flow.

Synthesis. Colloidal TM/ZnO nanoparticles were synthesized by a nonhydrolytic alcoholysis ester elimination reaction of metal carboxylate precursors. In a typical preparation of $Zn_{0.95}Co_{0.05}O$ nanocrystals, anhydrous zinc acetate (0.073 g, 0.4 mmol) and anhydrous cobalt acetate (0.0037 g, 0.021 mmol) were loaded in a 50 mL three-neck flask with 0.5 mL (∼1.5 mmol) of oleic acid and 4.0 mL (∼12 mmol) of oleyl alcohol. The reaction flask was evacuated to a vacuum level of 2 mbar for 30 min at 100 °C. The reaction system was then heated (∼10 °C min^{-1}) to 220 °C under argon flow and maintained at this temperature for 2 h. The solution was then cooled to 60 °C, and 5 mL of methanol was added to precipitate the nanocrystals. The crude product was recovered by centrifugation, dispersed in toluene, and subjected to a second round of purification. The obtained organic surfactant-coated nanocrystals could be easily redispersed in nonpolar solvents such as chloroform or toluene and used for further characterization without any size selection. Similarly, $Zn_{1-x}Co_xO$ ($x = 0.0$, 0.03, 0.07) and $Zn_{1-x}Ni_xO$ ($x = 0.02$, 0.03) were synthesized.

SCHEME 1

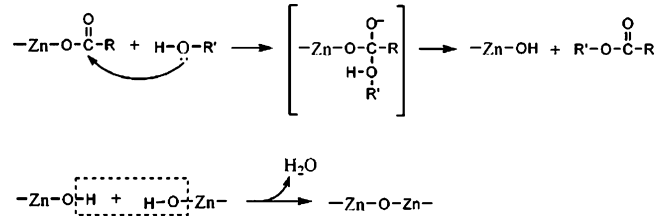

Characterization. The phase purity and structure of the nanocrystals were determined by X-ray powder diffraction data, which were collected on a Philips X'Pert pro X-ray diffractometer using monochromatized Cu Kα radiation ($\lambda = 1.5418$ Å) and operating at 40 kV and 30 mA. The synchrotron powder X-ray diffraction data was recorded in Debye−Scherrer mode using wavelengths 0.6888 Å (Co/ZnO) and 0.6825 Å (Ni/ZnO) at the Elettra synchrotron radiation (SR) source using a MAR 3475 image plate. The data was converted to a two-dimensional (2D) plot using Fit2D software.[31] The elemental composition of the prepared samples was confirmed by the ICP-AES (inductively coupled plasma atomic emission spectroscopy) analyses using a Jobin Yvon JY2000 spectrometer. Transmission electron (TEM) micrographs were obtained using a FEI-Tecnai G-20 microscope operating at 200 keV. The TEM specimens were prepared by dispersing the samples in ethanol and placing a drop of the dispersion on a Cu TEM grid covered with a holey carbon film, which was then dried. Micro-Raman spectra of the nanocrystals were obtained on a LABRAM-I, ISA make spectrometer using an Ar^+ ion laser (488 nm) equipped with a Peltier-cooled CCD detector. All the spectra were recorded in backscattering configuration. The dc magnetic measurements were carried out using a superconducting quantum interference device magnetometer (Quantum design, MPMS-XL). The optical absorption spectra were collected on a Jasco V-650 spectrophotometer.

Results and Discussion

Synthesis. Co- and Ni-doped ZnO nanocrystals have been conveniently synthesized by a nonhydrolytic alcoholysis route based on the well-known ester-elimination reaction that involves the nucleophilic attack of the hydroxyl group of alcohol on the carbonyl carbon atom of metal carboxylate derivatives[32] (Scheme 1).

Structural and Morphological Characterization Co-Doped ZnO Nanocrystals. The phase purity and crystal structure of the nanocrystals have been analyzed by X-ray diffraction (XRD) and Rietveld refinement of the diffraction data using the Fullprof2K software package.[33] All the diffraction peaks can be indexed to the wurtzite structure of ZnO (space group $P6_3mc$) (Figure 1a). There is no indication of any secondary phase or clusters, confirming that the samples are single phase. The lattice parameters of Co-doped ZnO calculated from XRD data are slightly smaller than those of undoped ZnO (Table S1, Supporting Information). The small decrease in lattice parameters is due to the substitution of slightly smaller Co^{2+} (0.58 Å) in place of Zn^{2+} (0.60 Å) in tetrahedral coordination of ZnO wurtzite structure. Similar small decrease in the lattice param-

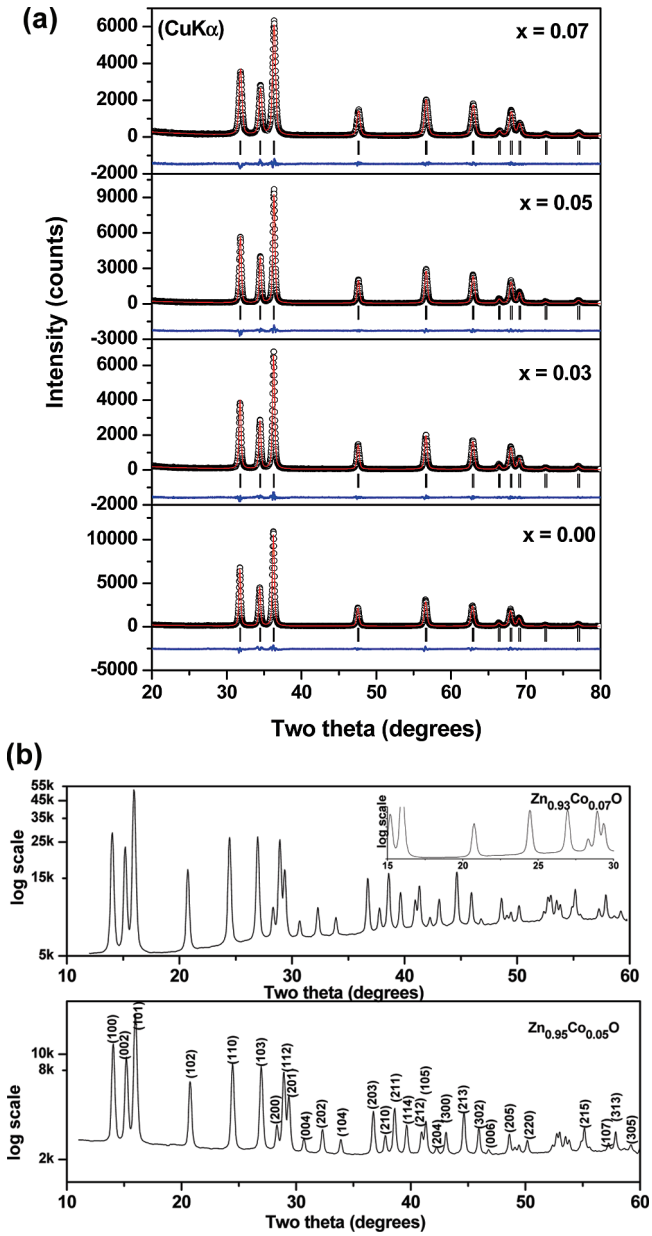

Figure 1. (a) Rietveld-refined XRD data of $Zn_{1-x}Co_xO$ ($x = 0.0$, 0.03, 0.05, 0.07) nanocrystals. The dots represent the observed data, whereas the solid line through the dots is the calculated profile; vertical tics below curves represent Bragg reflections for the phase. The difference pattern is given below the vertical tics. (b) XRD patterns of $Zn_{1-x}Co_xO$ ($x = 0.05$, 0.07) nanocrystals recorded using a synchrotron radiation source. The inset expands the 15−30° region for $Zn_{0.93}Co_{0.07}O$ nanocrystals.

eters on Co addition in ZnO has been reported previously also.[34] It may be mentioned here that if Co^{2+} ions were present in the octahedral environment, it would be signaled by significant increase in cell volume as octahedral Co^{2+} has an ionic radius of either 0.65 Å (low spin) and of 0.74 Å (high-spin state).[35] It is to be noted that Co^{3+} ion, though of smaller ionic radius, does not readily prefer the tetrahedral coordination.[35]

To further confirm the absence of any secondary phase, powder XRD data for $Zn_{1-x}Co_xO$ ($x = 0.5$, 0.7) nanocrystals were recorded using a synchrotron radiation source (Figure 1b and Figure S1, Supporting Information). The enhanced signal-to-noise ratio of the data confirms the absence of any hidden secondary phase in the samples. The profiles of the diffraction data were analyzed by Fullprof2K software, and the refined powder XRD data for these two compositions are shown in Figure 1b. It is also observed that the tetrahedral ZnO_4 unit remains undistorted with the Co substitution, except that there is a subtle reduction of the apical Zn−O bond from 1.967 (in $x = 0.5$) to 1.960 Å (in $x = 0.7$). The reduction is in accordance with the decrease in unit cell parameters of the $Zn_{1-x}Co_xO$ compositions. The other Zn−O bonds are 1.981(1) for ($x = 0.5$) and 1.983 Å for ($x = 0.7$).

The average concentration of the cobalt in Co-doped ZnO nanocrystals has been determined with ICP-AES, and the values are 2.36, 4.72, and 6.26 atom % for $Zn_{0.97}Co_{0.03}O$, $Zn_{0.95}Co_{0.05}O$, and $Zn_{0.93}Co_{0.07}O$ nanocrystals, respectively.

The morphology and further structural characterization of the nanocrystals has been carried out using TEM. The TEM images for a representative sample, $Zn_{0.95}Co_{0.05}O$, are shown in Figure 2. The nanocrystals have nearly spherical shapes and the average diameter in the range of 20−23 nm. The absence of any impurity phase such as metallic Co clusters or cobalt oxides (CoO or CO_3O_4) in the nanosize range has been further confirmed by selected area electron diffraction (SAED) studies (Figure 2b). The SAED pattern of the nanocrystals features ring patterns assigned to (100), (002), (101), (102), (110), and (103) planes and proves the high crystallinity of the nanocrystals. The high-resolution (HR) TEM image of a single nanocrystal (Figure 2c) shows well-defined lattice planes, indicating the single-crystalline nature of the nanoparticles. The lattice spacing of ∼2.60 Å observed throughout the HRTEM image corresponds to (002) interplanar distance of wurtzite ZnO. TEM images of the other $Zn_{1-x}Co_xO$ ($x = 0.0$, 0.03, 0.07) nanocrystals are shown in Figure S2, Supporting Information.

Structural Characterization of Ni-Doped ZnO Nanocrystals. Figure 3 shows the powder XRD patterns of the $Zn_{1-x}Ni_xO$ ($x = 0.02$, 0.03) nanocrystals recorded using a synchrotron radiation source. In both 2% and 3% Ni-doped ZnO samples very weak reflections arising from NiO and Ni metal are observed (inset, Figure 3). The metallic Ni precipitates increase as the dopant level increases from 2% to 3%. The unit cell parameters show decreasing trend as observed in the case of Co-doped ZnO nanocrystals (Table S2, Supporting Information); however, the presence of segregated NiO or Ni indicates that the solubility limit of Ni in ZnO is below 2 mol %. Quantitative estimation by Rietveld refinement of powder X-ray data of $Zn_{0.97}Ni_{0.03}O$ nanocrystals reveals that the segregated Ni and NiO phases are about 0.5 and 0.8 wt %, respectively. The average crystallite size as determined using Scherrer's formula ($t = K\lambda/B \cos\theta$, where t = average crystallite size in Å, K = Scherrer constant usually taken as 0.9 Å, λ = X-ray wavelength, θ is the Bragg angle, and B = integral breadth of a reflection located at 2θ) range from 20 to 24 nm for $Zn_{1-x}Ni_xO$ nanocrystals.

Local TM Dopant Structure in TM-Doped ZnO Nanocrystals. The valence state and substitution of Co^{2+} in ZnO nanocrystals has been examined with optical absorption spectroscopy. Figure 4a shows the room-temperature UV−vis spectrum of colloidal $Zn_{0.95}Co_{0.05}O$ nanocrystals. The band gap transition of the host ZnO NCs is observed as a shoulder at ∼350 nm. The band gap energy is estimated from the absorption spectrum to be ca. 385 nm (∼3.2 eV) similar to the band gap energy of bulk ZnO. Since the Bohr radius of ZnO is ca. 1.8 nm,[36] which is significantly smaller than the average radius of the NCs obtained in this work, strong quantum confinement effects are not expected. The absorption spectrum of the concentrated suspension of the same nanocrystals reveals three transitions at ∼565, 610, and 650 nm which can be readily

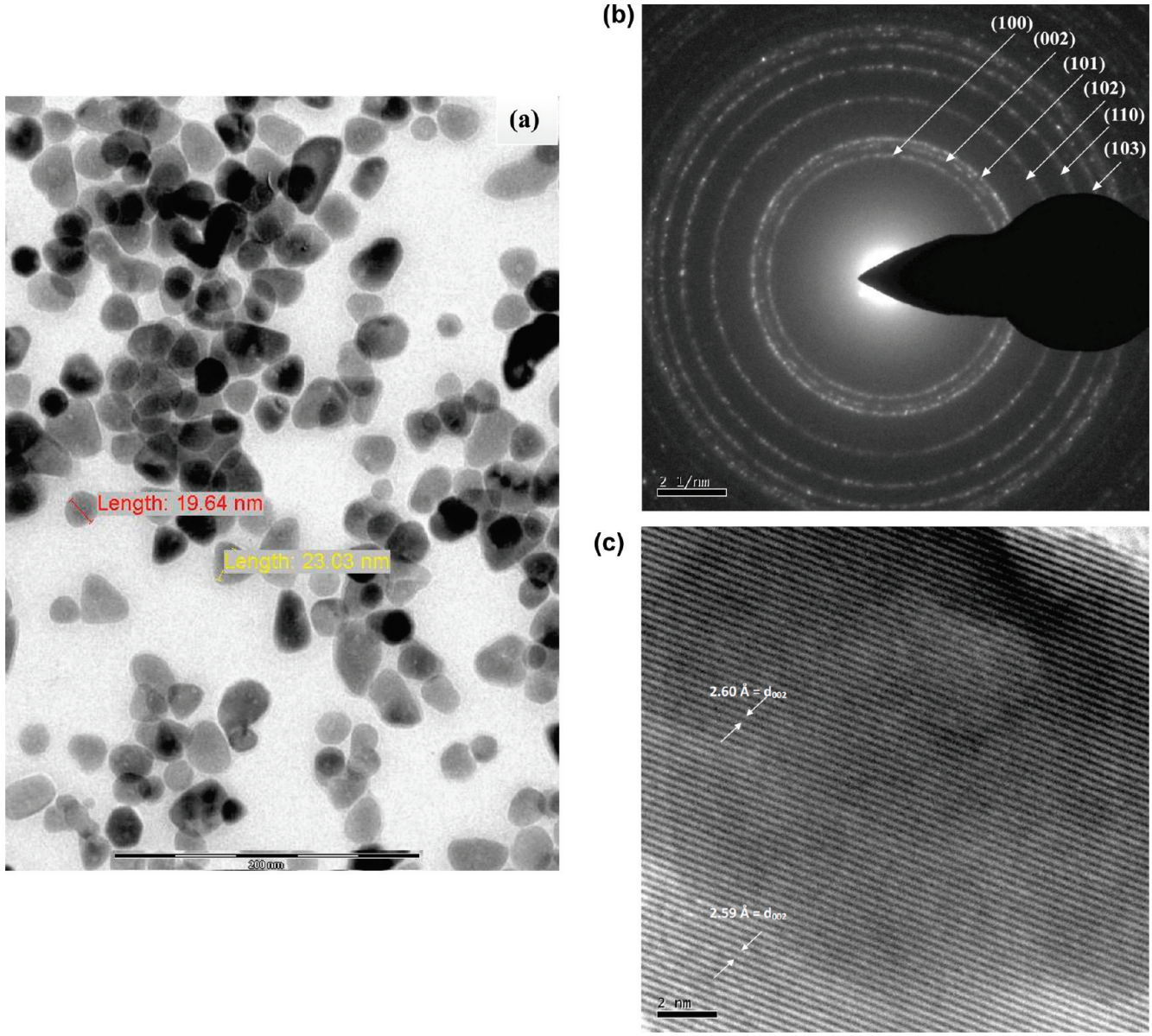

Figure 2. TEM (a), SAED (b), and HRTEM (c) images of $Zn_{0.95}Co_{0.05}O$ nanocrystals.

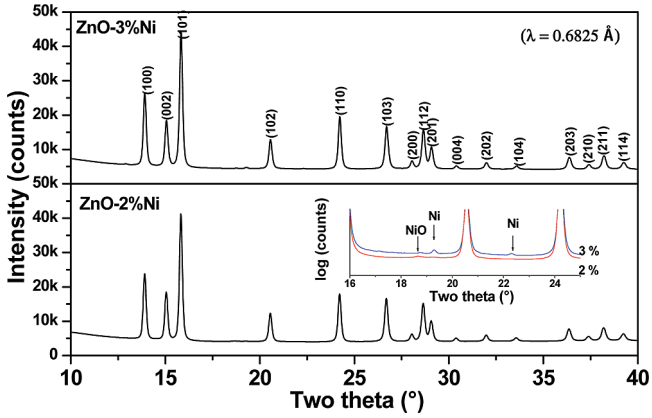

Figure 3. XRD patterns of $Zn_{1-x}Ni_xO$ ($x = 0.02$, 0.03) nanocrystals recorded using a synchrotron radiation source.

assigned to $^4A_2(F) \rightarrow {}^2A_1(G)$, $^4A_2(F) \rightarrow {}^4T_1(P)$, and $^4A_2(F) \rightarrow {}^2E_1(G)$ ligand field transitions, respectively, of tetrahedral Co^{2+} in tetrahedral symmetry.[37] A Co^{2+} cation is in $3d^7$ configuration, and according to Hund's rule and Pauli's exclusion principle, its electronic ground-state configuration has $L = 3$ and $S = {}^3/_2$. So, the ground-state spectral term is ^4F and the excited state terms are ^4P, ^2G, ^2F, ^2D, and ^2P.[38] However, when the Co^{2+} exists in the tetrahedral field, the ^4F term splits into $^4A_2$ (F), $^4T_2$ (F), and $^4T_1$ (F), with $^4A_2$ (F) being lowest in energy and the remaining two having higher energies. The ^4P term corresponding to the first excited state does not split but is transformed into $^4T_1$ (P). Similarly, ^2G splits into $^2A_1$ (G), ^2E (G), $^2T_1$ (G), and $^2T_2$ (G). In the ground state, the atom is in the $^4A_2$ state. When the electron has sufficient energy, it can be excited to higher energy states. The observation of these transitions in the absorption spectra of $Zn_{0.95}Co_{0.05}O$ nanocrystals clearly reveals that the added cobalt atoms have substituted Zn^{2+} cations and are present in the +2 state.

The partial incorporation of Ni^{2+} in ZnO has been confirmed from electronic absorption spectroscopy. Figure 4b shows the electronic absorption spectrum of $Zn_{0.98}Ni_{0.02}O$ nanocrystals. The absorption spectrum of the concentrated solution of the same nanocrystals reveals a spin−orbit split $^3T_1(F) \rightarrow {}^3T_1(P)$ ligand field transition of substitutionally doped tetrahedral Ni^{2+} ions at ~637 nm, which matches the corresponding transition in bulk

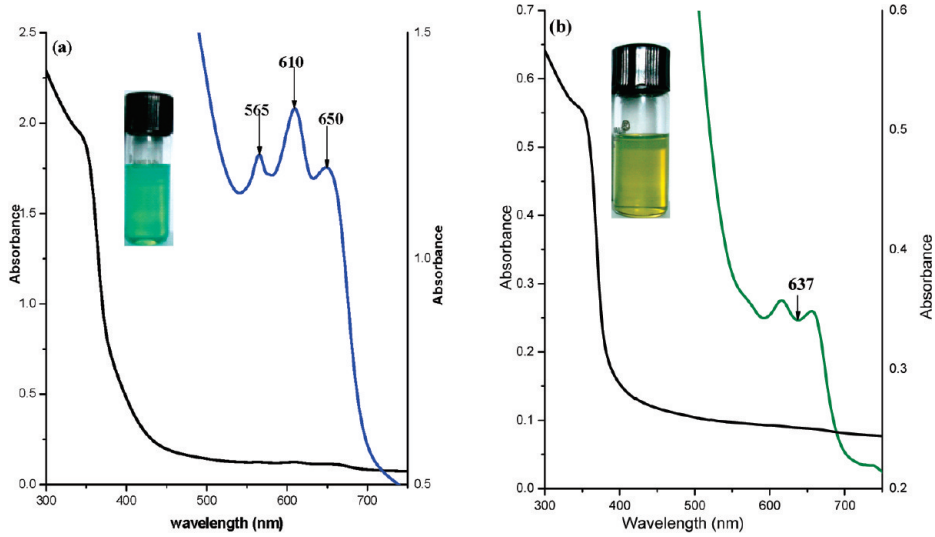

Figure 4. Optical absorption spectra of (a) colloidal $Zn_{0.95}Co_{0.05}O$ and (b) $Zn_{0.98}Ni_{0.02}O$ nanocrystals recorded at room temperature. Ligand field transitions of Co^{2+}/Ni^{2+} are collected on ca. 50 times concentrated nanocrystal suspensions (inset: photographs of colloidal $Zn_{1-x}TM_xO$ nanocrystals dispersed in chloroform).

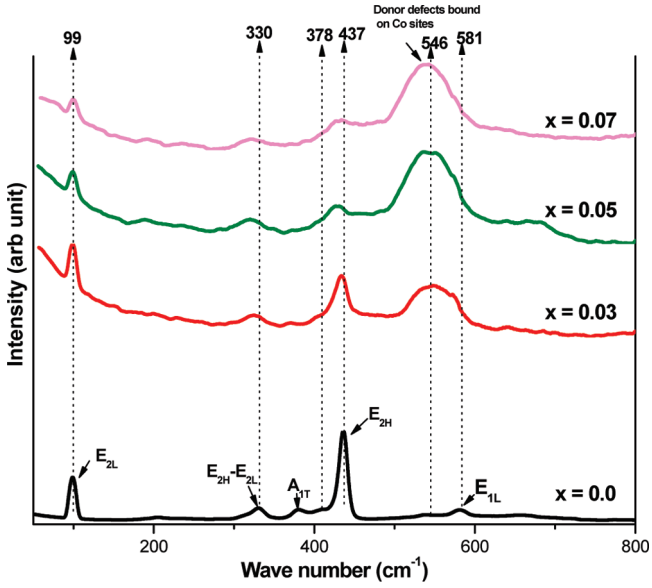

Figure 5. Room-temperature micro-Raman spectra of $Zn_{1-x}Co_xO$ (x = 0.0, 0.03 0.05, 0.07) nanocrystals.

single crystal of Ni-doped ZnO, indicating partial incorporation of Ni into the host lattice.[24,37]

Raman Spectroscopy of Co-Doped ZnO Nanoparticles. Raman spectroscopy is a versatile technique for detecting dopant incorporation and the resulting defects and lattice disorder in a host lattice.[39] In particular, micro-Raman spectroscopy has proven to be a very sensitive technique to detect secondary phases in TM-implaned ZnO materials.[40] The wurtzite ZnO has six Raman-active phonon modes at 101 (E_2 low), 381 (A_1 TO), 407 (E_1 TO), 437 (E_2 high), 574 (A_1 LO), and 583 cm^{-1} (E_1 LO) of first order, respectively.[41] Figure 5 shows the composition-dependent room-temperature micro-Raman spectra of $Zn_{1-x}Co_xO$ nanocrystals. It is clear from the data that all the prominent peaks of ZnO are also observed in Co-doped nanocrystals, but the Raman modes in Co-doped ZnO nanoparticles are broad, relatively less intense, and shifted toward lower frequencies as the Co content in the $Zn_{1-x}Co_xO$ nanocrystals increases from 0 to 0.07. These observations reveal that the local symmetry in the nanocrystals is different from that of bulk, but the crystal structure is the same in both. The sharpest and strongest peak at about 437 cm^{-1} can be assigned to the high-frequency branch of E_2 high mode (E_{2H}), which involves the oxygen motion and is characteristic of wurtzite structure.[41] The pronounced red-shift, broadening, and weakening of the nonpolar E_{2H} mode for the doped ZnO samples, as compared to pure ZnO, are the consequence of the structural defect formation and local lattice distortions induced by doping.[9c] The peak at about 330 cm^{-1} is assigned as a difference mode between the E_2 high and E_2 low frequencies.[42] In comparison to the Raman spectrum of pure ZnO[41] the additional mode around 546 cm^{-1} can be assigned to the quasi-longitudinal-optical (LO) phonon mode, due to the abundant shallow donor defects, such as zinc interstitials and/or oxygen vacancies, bound on the tetrahedral Co sites.[9c,43] Further, no additional Raman modes due to either cobalt oxides (CoO/Co_3O_4) or $ZnCo_2O_4$ are observed[44] for $Zn_{1-x}Co_xO$ nanocrystals as x changes from 0 to 0.07, revealing the absence of any impurity phase.

Magnetic Properties of Co-Doped ZnO Nanocrystals. The magnetic properties of the $Zn_{1-x}Co_xO$ (x = 0.05, 0.07) are shown in Figure 6. The samples exhibit well-defined hysteresis loops at 300 K, which is indicative of room-temperature ferromagnetic behavior. In contrast, the undoped ZnO and 3% Co-doped samples prepared under similar reaction conditions show diamagnetic behavior (Figure S3, Supporting Information). The maximum moments have been deduced to be 0.074 and 0.049 μ_B/Co^{2+} (μ_B: Bohr magneton) with corresponding coercivities of 450 and 320 Oe (1 Oe = 79.57747 A m^{-1}) for $Zn_{0.95}Co_{0.05}O$ and $Zn_{0.93}Co_{0.07}O$ nanocrystals, respectively. The decrease of maximum moment for the x = 0.07 sample is inconsistent with a scenario involving FM from the segregation of secondary phases such as metallic Co, suggesting that the observed room-temperature FM is an intrinsic property.

Temperature-dependent magnetization of x = 0.05 and 0.07 samples under zero-field cooling (ZFC) and field cooling (FC) at 100 Oe between 5 and 300 K is depicted in Figure 7. There is a clear divergence between the FC and ZFC curves around 300 K, indicating that the systems are ferromagnetic at room temperature (RT). The steep increase of magnetization with decreasing temperatures below 25 K in the magnetization is characteristic of all DMS materials and is probably related to the defect structure and possible fraction of weakly coupled/

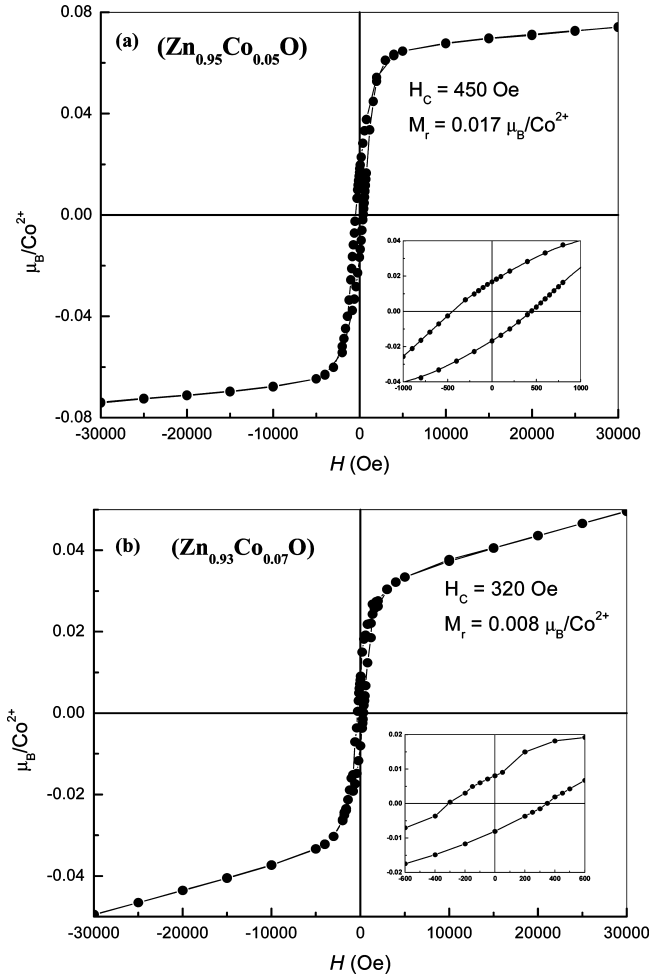

Figure 6. Magnetization (M) as a function of applied field (H) at 300 K for (a) $Zn_{0.95}Co_{0.05}O$ and (b) $Zn_{0.93}Co_{0.07}O$ nanocrystals. Insets expand the lower field region to show the presence of remanence and coercivity.

uncoupled Co^{2+} ions.[24,45] Above 25 K the magnetization under ZFC increases monotonically with increasing temperature, indicating that there are no Co metallic nanoclusters, otherwise they should display the superparamagnetic behavior below 300 K.[46] The magnetization under FC decreases with decreasing temperature, which is very different from FC curves for noninteracting magnetic nanoparticles.[47] On the basis of SRXRD, Raman, and HRTEM data, the presence of any secondary phases such as metallic Co and cobalt oxides (CoO or Co_3O_4) may be ruled out. Therefore, in $Zn_{1-x}Co_xO$ ($x = 0.05, 0.07$) nanocrystals

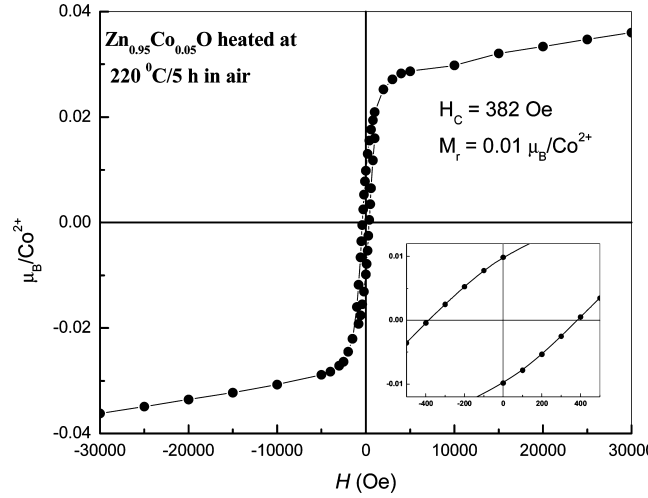

Figure 8. Magnetization (M) as a function of applied field (H) for $Zn_{0.95}Co_{0.05}O$ nanocrystals at RT after annealing in air at 220 °C for 5 h.

the ferromagnetism is expected to arise from the intrinsic exchange interaction of magnetic moments in doped nanocrystals.

The observed ferromagnetism in ZnO/Co nanocrystals is explained on the basis of bound magnetic polaron mechanism,[27] discussed earlier. In the framework of this theory, not only the dopant concentration but also the number of donor electrons must be quite large to obtain ferromagnetism. Lower values of coercivity ($H_C = 382$ Oe) and remanence ($M_r = 0.01\ \mu_B/Co^{2+}$) observed in $Zn_{0.95}Co_{0.05}O$ nanocrystals annealed in O_2 atmosphere for 5 h at 220 °C (Figure 8) indicate that oxygen vacancies do play a part to get a ferromagnetic coupling of the magnetic spins. The annealed sample was analyzed by X-ray diffraction, and it was found that the structure remains unmodified, implying that only the defects structure of the samples is varied upon annealing. In the case of O_2 annealing, the most plausible effect is the annihilation of intrinsic oxygen vacancies.[48] However, another possibility is that annealing in O_2 atmosphere may cause either the out-diffusion or passivation of Zn interstials due to the formation of a donor−acceptor pair of interstitial zinc and interstitial oxygen resulting in lower magnetization values. The annihilation of Zn_i on annealing in O_2 atmosphere is well-documented in literature.[49] The donor defects bound to Co sites have been observed by Raman spectroscopy in the present case. In light of the above facts, we believe that the donor defects play a crucial role in mediating the high-temperature FM in Co-doped ZnO nanocrystals, and thus detailed investigation into the nature of these defects will be beneficial in understanding the origin of FM.

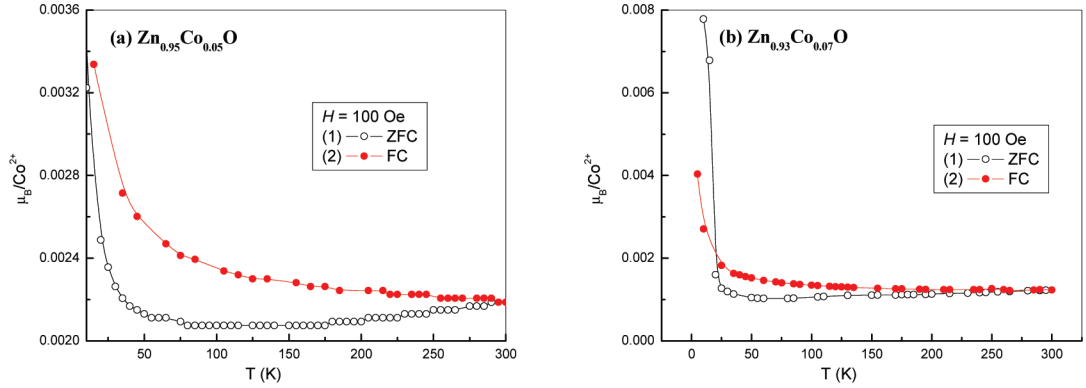

Figure 7. ZFC and FC magnetization curves for (a) $Zn_{0.95}Co_{0.05}O$ and (b) $Zn_{0.93}Co_{0.07}O$ nanocrystals at an external applied field of 100 Oe.

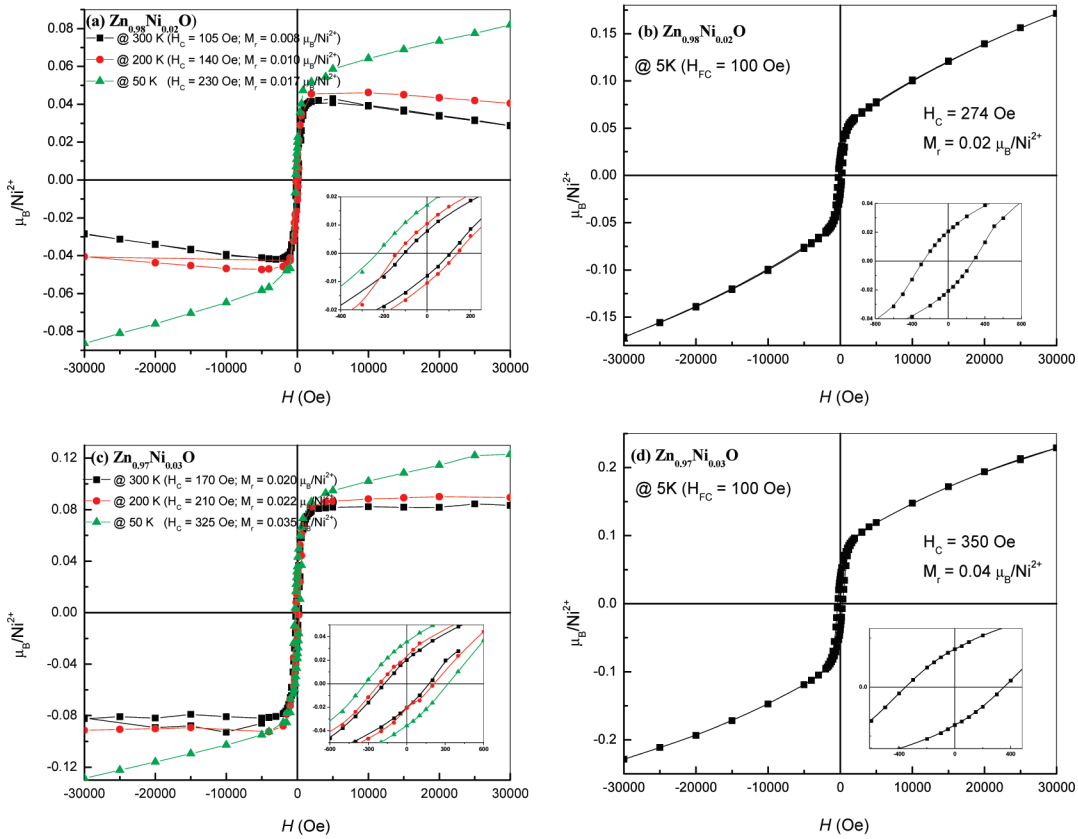

Figure 9. Magnetization (M) as a function of applied field (H) for $Zn_{1-x}Ni_xO$ nanocrystals. Insets expand the lower field region to show the presence of remanence and coercivity.

TABLE 1: Coercivity (H_C), Maximum Magnetization (M_s), and Remanence (M_r) Values of $Zn_{1-x}Ni_xO$ Nanocrystals

system	T (K)	H_C (Oe)	M_s (μ_B/Ni^{2+})	M_r (μ_B/Ni^{2+})
$Zn_{0.98}Ni_{0.02}O$	5	274	0.171	0.020
	50	230	0.082	0.017
	200	140	0.040	0.010
	300	105	0.029	0.008
$Zn_{0.97}Ni_{0.03}O$	5	350	0.229	0.04
	50	325	0.123	0.035
	200	210	0.089	0.022
	300	170	0.083	0.020

Magnetization Properties of Ni-Doped ZnO Nanocrystals. Magnetization (M) versus (H) plots for $Zn_{1-x}Ni_xO$ nanocrystals are shown in Figure 9, and the plots indicate the ferromagnetic nature of the nickel-doped zinc oxide nanocrystals in the temperature range of 5−300 K. The values of their coercive field, maximum moments observed, and remanence at different temperatures are summarized in Table 1. The values of all the parameters (H_C, M_s, and M_r) decrease with increasing temperature but increase with increasing Ni content. Accordingly, the maximum moment observed for the two compositions lies between 0.17 and 0.23 μ_B/Ni^{2+} at 5 K and increases with increasing Ni content. The coercivity values (H_C) also increase with the nickel content, being 274 and 320 Oe for $Zn_{0.98}Ni_{0.02}O$ and $Zn_{0.97}Ni_{0.03}O$ nanocrystals, respectively. At RT, the values of the maximum moment are 0.029 and 0.083 μ_B/Ni^{2+} for $Zn_{0.98}Ni_{0.02}O$ and $Zn_{0.97}Ni_{0.03}O$ nanocrystals, respectively. The temperature dependence of the magnetization has been investigated for both ZFC and FC conditions for H = 100 Oe, and the results are shown in Figure 10. The $M-T$ results clearly show that the prepared samples maintain the ferromagnetic ordering at room temperature. Very similar ZFC−FC curves have been reported by Park et al.[13a] for Co-doped ZnO thin films, where the observed irreversibility between ZFC−FC is due to the presence of nanometer-sized Co clusters. On the basis of this observation and SRXRD data, we believe that the observed room-temperature ferromagnetism in Ni-doped ZnO nanocrystals arises from secondary phases, mainly Ni clusters.

Conclusions

A facile chemical synthesis for dispersible Co- and Ni-doped ZnO nanocrystals ($Zn_{1-x}TM_xO$ where x = 0−0.07 for TM = Co and x = 0.02, 0.03 for TM = Ni) has been developed based on nonhydrolytic alcoholysis ester elimination reaction using anhydrous metal carboxylates as precursors in the presence of oleic acid and oleyl alcohol at 220 °C. The single-phase structure in the case of Co-doped ZnO has been confirmed by detailed XRD, microstructure, and Raman studies. On the other hand, in the powder XRD patterns of Ni-doped ZnO nanocrystals, other phases like NiO and Ni could be seen. TM-doped ZnO nanocrystals are ferromagnetic at room temperature. The observed ferromagnetism in ZnO/Co nanocrystals is explained on the basis of bound magnetic polaron mechanism and is likely to be donor defects (V_O/Zn_i) mediated. The observed ferromagnetism in Ni-doped ZnO nanocrystals seems to originate mainly from Ni clusters. The synthetic method employed can also be extended to prepare other semiconducting oxide nanocrystals doped with transition metal ions.

Supporting Information Available: Tables of refined unit cell parameters of various $Zn_{1-x}TM_xO$ (TM = Co, Ni) compositions, SRXRD plots of $Zn_{1-x}Co_xO$ (x = 0.03, 0.07) nanocrystals, TEM images of $Zn_{1-x}Co_xO$ (x = 0.0, 0.03, 0.07) nanocrystals, magnetization (M) vs applied field (H) for pure ZnO and

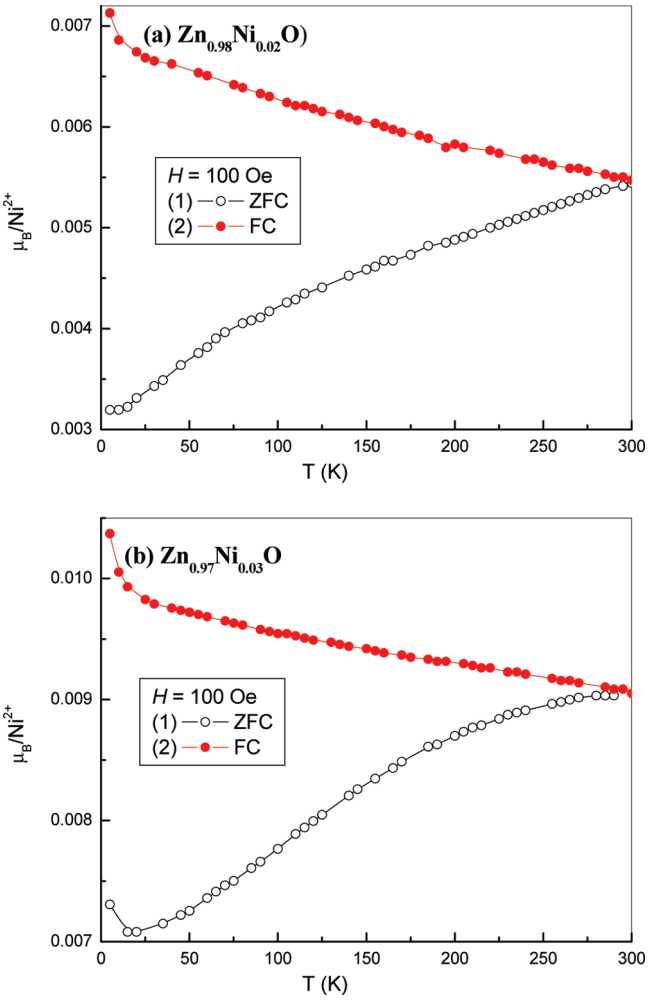

Figure 10. ZFC and FC magnetization curves for (a) $Zn_{0.98}Ni_{0.02}O$ and (b) $Zn_{0.97}Ni_{0.03}O$ nanocrystals at an external applied field of 100 Oe.

$Zn_{0.97}Co_{0.03}O$ nanocrystals. This material is available free of charge via the Internet at http://pubs.acs.org.

References and Notes

(1) Furdyna, J. K., Kossut, J., Eds.; *Diluted Magnetic Semiconductors (Semiconductors and Semimetals)*; Academic: New York, 1988; Vol. 25.

(2) (a) Wolf, S. A.; Awschalom, D. D.; Buhrman, R. A.; Daughton, J. M.; von Molnár, S.; Roukes, M. L.; Chtchelkanova, A. Y.; Treger, D. M. *Science* **2001**, *294*, 1488. (b) Ohno, H.; Matsukura, F.; Ohno, Y. *JSAP Int.* **2002**, *5*, 4.

(3) Bhatti, K. P.; Kundu, S.; Chaudhary, S.; Kashyap, S. C.; Pandya, D. K. *J. Phys. D: Appl. Phys.* **2006**, *39*, 4909.

(4) Pearton, S. J.; Abernathy, C. R.; Overberg, M. E.; Thaler, G. T.; Norton, D. P.; Theodoropoulou, N.; Hebard, A. F.; Park, Y. D.; Ren, F.; Kim, J.; Boatner, L. A. *J. Appl. Phys.* **2003**, *93*, 1.

(5) Ando, K. In *Solid-State Sciences: Magneto-Optics*; Sugano, S., Kojima, N., Eds.; Springer: New York, 2000; Vol. 128, p 211.

(6) (a) Dietl, T.; Ohno, H.; Matsukura, F.; Cibert, J.; Ferrand, D. *Science* **2000**, *287*, 1019. (b) Sato, K.; Katayama-Yoshida, H. *Physica E* **2001**, *10*, 251.

(7) Ueda, K.; Tabata, H.; Kawai, T. *Appl. Phys. Lett.* **2001**, *79*, 988.

(8) Lee, H.-J.; Jeong, S. Y.; Cho, C. R.; Park, C. H. *Appl. Phys. Lett.* **2002**, *81*, 4020.

(9) (a) Ramachandran, S.; Tiwari, A.; Narayan, J. *Appl. Phys. Lett.* **2004**, *84*, 5255. (b) Deka, S.; Pasricha, R.; Joy, P. A. *Chem. Mater.* **2004**, *16*, 1168. (c) Wang, X.; Xu, J.; Zhang, B.; Yu, H.; Wang, J.; Zhang, X.; Yu, J.; Li, Q. *Adv. Mater.* **2006**, *18*, 2476.

(10) (a) Venkatesan, M.; Fitzgerald, C. B.; Lunney, J. G.; Coey, J. M. D. *Phys. Rev. Lett.* **2004**, *93*, 177206. (b) Fitzgerald, C. B.; Venkatesan, M.; Lunney, J. G.; Dorneles, L. S.; Coey, J. M. D. *Appl. Surf. Sci.* **2005**, *247*, 493.

(11) Dinia, A.; Schmerber, C.; Meny, C.; Pierron-Bohnes, V.; Beaurepaire, E. *J. Appl. Phys.* **2005**, *97*, 123908.

(12) (a) Jin, Z.; Fukumara, T.; Kawasaki, M.; Ando, K.; Saito, H.; Sekiguchi, T.; Yoo, Y. Z.; Murakami, M.; Matsumoto, Y.; Hasegawa, T.; Koinuma, H. *Appl. Phys. Lett.* **2001**, *78*, 3824. (b) Lawes, G.; Risbud, A. S.; Ramirez, A. P.; Seshadri, R. *Phys. Rev. B* **2005**, *71*, 45201. (c) Shi, T.; Zhu, S.; Sun, Z.; Wei, S.; Liu, W. *Appl. Phys. Lett.* **2007**, *90*, 102108. (d) Rao, C. N. R.; Deepak, F. L. *J. Mater. Chem.* **2005**, *15*, 573. (e) Spaldin, N. A. *Phys. Rev. B* **2004**, *69*, 125201. (f) Lojkowski, W.; Gedanken, A.; Grzanka, E.; Opalinska, A.; Strachowski, T.; Pielaszek, R.; Tomaszewska-Grzeda, A.; Yatsunenko, S.; Godlewski, M.; Matysiak, H.; Kurzydłowski, K. J. *J. Nanopart. Res.* **2009**, *11*, 1991.

(13) (a) Park, J. H.; Kim, M. G.; Jang, H. M.; Ryu, S.; Kim, Y. M. *Appl. Phys. Lett.* **2004**, *84*, 1338. (b) Kim, J. H.; Kim, H.; Kim, D.; Ihm, Y. E.; Choo, W. K. *J. Appl. Phys.* **2002**, *92*, 6066.

(14) Schwartz, D. A.; Norberg, N. S.; Nguyen, Q. P.; Parker, J. M.; Gamelin, D. R. *J. Am. Chem. Soc.* **2003**, *125*, 13205.

(15) (a) Gacic, M.; Jakob, G.; Herbort, C.; Adrian, H.; Tietze, T.; Bruck, S.; Goering, E. *Phys. Rev. B* **2007**, *75*, 205206. (b) Barla, A.; Schmerber, G.; Beaurepaire, E.; Dinia, A.; Bieber, H.; Colis, S.; Scheurer, F.; Kappler, J. P.; Imperia, P.; Nolting, F.; Wilhelm, F.; Rogalev, A.; Müller, D.; Grob, J. J. *Phys. Rev. B* **2007**, *76*, 125201.

(16) Tuan, A. C.; Bryan, J. D.; Pakhomov, A. M.; Shutthanandan, V.; Thevuthasan, S.; McCready, D. E.; Gaspar, D.; Engelhard, M. H.; Rogers, J. W., Jr.; Krishnan, K.; Gamelin, D. R.; Chambers, S. A. *Phys. Rev. B* **2004**, *70*, 054424.

(17) (a) Schwartz, D. A.; Gamelin, D. R. *Adv. Mater.* **2004**, *16*, 2115. (b) Khare, N.; Kappers, M. J.; Wei, M.; Blamire, M. G.; Macmanus-Driscoll, J. L. *Adv. Mater.* **2006**, *18*, 1449.

(18) Coey, J. M. D.; Venkatesan, M.; Stamenov, P.; Fitzgerald, C. B.; Dorneles, L. S. *Phys. Rev. B* **2005**, *72*, 024450.

(19) Wakano, T.; Fujimura, N.; Morinaga, Y.; Abe, N.; Ashida, A.; Ito, T. *Physica E* **2001**, *10*, 260.

(20) Yin, Z. G.; Chen, N.; Yang, F.; Chai, S. L.; Zhong, J.; Qian, H. J.; Ibrahim, K. *Solid State Commun.* **2005**, *135*, 430.

(21) Jung, S. W.; Park, W. I.; Yi, G.-C.; Kim, M. Y. *Adv. Mater.* **2003**, *15*, 1358.

(22) Cui, J. B.; Gibson, U. J. *Appl. Phys. Lett.* **2005**, *87*, 133108.

(23) Radovanovic, P V.; Gamelin, D. R. *Phys. Rev. Lett.* **2003**, *91*, 157202.

(24) Schwartz, D. A.; Norberg, N. S.; Nguyen, Q. P.; Parker, J. M.; Gamelin, D. R. *J. Am. Chem. Soc.* **2003**, *125*, 13205.

(25) Schwartz, D. A.; Kittilstved, K. R.; Gamelin, D. R. *Appl. Phys. Lett.* **2004**, *85*, 1395.

(26) Pearton, S. J.; Heo, W. H.; Ivill, M.; Norton, D. P.; Steiner, T. *Semicond. Sci. Technol.* **2004**, *19*, R59.

(27) (a) Coey, J. M. D.; Venkatesan, M.; Fitzgerald, C. B. *Nat. Mater.* **2005**, *4*, 173. (b) Coey, J. M. D. *J. Appl. Phys.* **2005**, *97*, 10D313.

(28) (a) Awschalom, D. D.; Flatté, M. E.; Samarth, N. *Sci. Am.* **2002**, *286*, 66. (b) Fiederling, R.; Keim, M.; Reuscher, G.; Ossau, W.; Schmidt, G.; Waag, A.; Molenkamp, L. W. *Nature* **1999**, *402*, 787. (c) Jonker, B. T.; Park, Y. D.; Bennett, B. R.; Cheong, H. D.; Kioseoglou, G.; Petrou, A. *Phys. Rev. B* **2000**, *62*, 8180.

(29) Ouyang, M.; Awschalom, D. D. *Science* **2003**, *301*, 1074.

(30) Songsheng, Q.; Ying, F.; Ruili, Y.; Liangchao, L. *Thermochim. Acta* **1997**, *303*, 47.

(31) Hammersley, A. P.; Svensson, S. O.; Hanfland, M.; Fitch, A. N.; Hausermann, D. *High-Pressure Res.* **1996**, *14*, 235.

(32) (a) Joo, J.; Kwon, S. G.; Yu, J. H.; Hyeon, T. *Adv. Mater.* **2005**, *17*, 1873. (b) Zhong, X.; Feng, Y.; Zhang, Y.; Lieberwirth, I.; Knoll, W. *Small* **2007**, *3*, 1194.

(33) Rodriguez-Carvajal, J. *Physica B* **1992**, *192*, 55.

(34) Yan, L.; Ong, C. K.; Rao, X. S. *J. Appl. Phys.* **2004**, *96*, 508.

(35) Shannon, R. D.; Prewitt, C. T. *Acta Crystallogr., Sect B* **1969**, *25*, 925.

(36) Sun, Y.; Ketterson, J. B.; Wong, G. K. L. *Appl. Phys. Lett.* **2000**, *77*, 2322.

(37) (a) Weakliem, H. A. *J. Chem. Phys.* **1962**, *36*, 2117. (b) Koidl, P. *Phys. Rev. B* **1977**, *15*, 2493.

(38) Lee, J. D. *Concise Inorganic Chemistry*, 5th ed.; ELBS with Chapman and Hall: London, 1996; p 947.

(39) Wang, J. B.; Huang, G. J.; Zhong, X. L.; Sun, L. Z.; Zhou, Y. C.; Liu, E. H. *Appl. Phys. Lett.* **2006**, *88*, 252502.

(40) Schumm, M.; Koerdel, M.; Müller, S.; Ronning, C.; Dynowska, E.; Gołacki, Z.; Szuszkiewicz, W.; Geurts, J. *J. Appl. Phys.* **2009**, *105*, 083525.

(41) (a) Damen, T. C.; Porto, S. P. S.; Tell, B. *Phys. Rev.* **1966**, *142*, 570. (b) Arguello, C. A.; Rousseau, D. L.; Porto, S. P. S. *Phys. Rev.* **1969**, *181*, 1351. (c) Calleja, J. M.; Cardona, M. *Phys. Rev. B* **1977**, *16*, 3753. (d) Wang, X.; Xu, J.; Yu, X.; Xue, K.; Yu, J.; Zhao, X. *Appl. Phys. Lett.* **2007**, *91*, 031908.

(42) Cuscó, R.; Alarcón-Lladó, E.; Ibáñez, J.; Artús, L. *Phys. Rev. B* **2007**, *75*, 165202.

(43) Schumm, M.; Koerdel, M.; Müller, S.; Zutz, H.; Ronning, C.; Stehr, J.; Hofmann, D. M.; Geurts, J. *New J. Phys.* **2008**, *10*, 043004.

(44) (a) Hadjiev, V. G.; Iliev, M. N.; Vergilov, I. V. *J. Phys. C: Solid State Phys.* **1988**, *21*, L199. (b) Gallant, D.; Pézolet, M.; Simard, S. *J. Phys. Chem. B* **2006**, *110*, 6871. (c) Zhang, Y. B.; Li, S.; Tan, T. T.; Park, H. S. *Solid State Commun.* **2006**, *137*, 142. (d) Samanta, K.; Bhattacharya, P.; Katiyar, R. S.; Iwamoto, W.; Pagliuso, P. G.; Rettori, C. *Phys. Rev. B* **2006**, *73*, 245213.

(45) Ohno, H.; Munekata, H.; Penney, T.; von Molnár, S.; Chang, L. L. *Phys. Rev. Lett.* **1992**, *68*, 2664.

(46) (a) Zhu, S.; Wang, L. M.; Zu, X. T.; Xiang, X. *Appl. Phys. Lett.* **2006**, *88*, 043107. (b) Wang, W.; Wang, Z.; Hong, Y.; Tang, J.; Yu, M. J. *Appl. Phys.* **2006**, *99*, 08M115.

(47) Zheng, R. K.; Gu, H. W.; Xu, B.; Zhang, X. X. *Phys. Rev. B* **2005**, *72*, 014416.

(48) (a) Vanheusden, K.; Seager, C. H.; Warren, W. L.; Tallant, D. R.; Voigt, J. A. *Appl. Phys. Lett.* **1996**, *68*, 403. (b) Vanheusden, K.; Warren, W. L.; Seager, C. H.; Tallant, D. R.; Voigt, J. A. *J. Appl. Phys.* **1996**, *79*, 7983.

(49) (a) Müller, S.; Lorenz, M.; Czekalla, C.; Benndorf, G.; Hochmuth, H.; Grundmann, M.; Schmidt, H.; Ronning, C. *J. Appl. Phys.* **2008**, *104*, 123504. (b) Müller, S.; Zhou, M.; Li, Q.; Ronning, C. *Nanotechnology* **2009**, *20*, 135704.

JP9105579